




Mapping subsurface defects and surface deformation along the artificial levee of the Lower Tisza River, Hungary

Díaa Sheishah^{1,2} · Tímea Kiss¹ · Tibor Borza³ · Károly Fiala³ · Péter Kozák³ · Enas Abdelsamei^{1,2} · Csaba Tóth⁴ · Gyula Grenczky⁵ · Dávid Gergely Páll¹ · György Sipos¹ 

Received: 11 October 2022 / Accepted: 15 March 2023 / Published online: 11 May 2023
© The Author(s) 2023

Abstract

Artificial levees along alluvial rivers are major components of flood-risk mitigation. This is especially true in the case of Hungary, where more than one-third of the country is threatened by floods and protected by an over 4200-km-long levee system. Most of such levees were built in the nineteenth century. Since then, several natural and anthropogenic processes, such as compaction and erosion, might have contributed to these earth structures' slow but steady deformation. Meanwhile, as relevant construction works were scarcely documented, the structure and composition of artificial levees are not well known. Therefore, the present analysis mapped structural differences, possible compositional deficiencies, and sections where elevation decrease is significant along a 40-km section of the Lower Tisza River. Investigations were conducted using real-time kinematic GPS and ground-penetrating radar (GPR). Onsite data acquisition was complemented with an analysis using a Persistent Scatterer Synthetic Aperture Radar to assess general surface deformation. GPR profiles showed several anomalies, including structural and compositional discontinuities and local features. The GPR penetration depth varied between 3 and 4 m. According to height measurements, the mean elevation of the levee crown decreased by 8 cm in 40 years. However, the elevation decrease reached up to 30 cm at some locations. Sections affected by structural anomalies, compositional changes, and increased surface subsidence are especially sensitive to floods when measurement results are compared with flood phenomena archives.

Keywords Tisza River · Levee health · Ground-penetrating radar · Surface deformation · Flood-risk

✉ György Sipos
gysipos@geo.u-szeged.hu

Extended author information available on the last page of the article

1 Introduction

Artificial levees are ultimately important earthworks for preventing flooding. Thus, knowing their conditions for successful flood protection is essential. Artificial levees, that is, linear manmade earthworks along rivers, have been built to inhibit the inundation of floodplains since historical times. However, large-scale construction works started at the turn of the nineteenth and twentieth centuries (Szűcs et al. 2019; Knox et al. 2022). These mixed-age structures were built using different techniques and materials (Tobin 1995).

In Hungary, more than one-third of the country is protected by an over 4200-km-long levee system, with some sections older than 150 years. These levees were constructed using compacted sediments. The least permeable sediments, such as clays, are placed at the riverside of the levee. The height of the levees is variable. The levees have been raised several times, but flood-risk is affected not only by their height but also by their composition, structure, and the various defects appearing in and on them. Because of their high age, we have limited information on their condition and changes through time (Ihrig 1973; Szűcs et al. 2019; Kiss et al. 2021). They were designed by considering many factors, such as the estimated flood stage, material type, types of land use and structures on the protected side, foundation, and the availability of land for construction (Lászlóffy 1982; Kiss et al. 2019).

The height of artificial levees, a key indicator for risk assessment, is widely monitored using various methods (Tanajewski and Bakula 2016; Kiss et al. 2021), but their internal structures remain hidden. As levees are critical and spatially extended infrastructure, the use of invasive and time-consuming techniques, usually providing only local information, is not a viable option for assessment. Consequently, geophysical methods generally can provide useful physical information on large areas with high accuracy. Such investigations depend on the contrast in physical properties between the anomaly and the surrounding soil. Shallow and nondestructive geophysical methods have widely been utilized recently in levee investigations (e.g., Perri et al. 2014; Busato et al. 2016; Sentenac et al. 2017; Borgatti et al. 2017; Rahimi et al. 2018; Dezert et al. 2019; Jodry et al. 2019; Tresoldi et al. 2019; Sheishah et al. 2022).

Electrical resistivity tomography (ERT) has been used by many authors to investigate the health of different levee sections along rivers and check their flood protection abilities. For instance, two-dimensional (2D) and three-dimensional (3D) ERT were utilized to locate fissures in embankments (Sentenac et al. 2012; Jones et al. 2014). Meanwhile, a 3D extended normalization approach of ERT was used in an embankment dike investigation (Fargier et al. 2014). ERT not only is adequate for structural assessments but also can enable the identification of seepage zones and sections affected by intensive water saturation through long-term monitoring, as demonstrated by Tresoldi et al. (2019) and Lee et al. (2020).

Active thermal sensing is used along with other geophysical techniques to detect leaks and erosion zones in levees (Radzicki et al. 2021). Using ERT enabled authors to assess the function between water content and resistivity values, which allowed the transformation of resistivity profiles into water content maps. Geotechnical investigations were also applied to validate geophysical surveys (Perri et al. 2014; Dezert et al. 2019). 2D DC ERT and seasonal temperature profiles were applied by Jodry et al. (2019) to monitor the seasonal change in soil moisture in an earthen levee to produce seasonal resistivity change models. Meanwhile, near-surface structures were mapped through the combined use of capacitive coupled resistivity and multichannel analysis of surface waves, and

information on potential problem areas along the levee could be provided (Rahimi et al. 2018). However, although ERT can reveal subsurface configurations and is commonly used for levee investigations, it still has some drawbacks. Different parameters, such as rainfall, temperature, sheet piling, and 3D effects can disturb ERT measurements (Fargier 2011; François et al. 2016). Furthermore, ERT requires high contrast in resistivity to provide promising results. Seismic surveys can also be used in levee investigations. However, if the contrast in acoustic impedance is not high enough, the levee structure could not be resolved (Karl et al. 2008). Also, if a heterogeneous material within the levee core is located below the resolution level, it cannot be easily detected.

On long sections, when fast, high-resolution data are necessary, ground-penetrating radar (GPR) provides the best solution (e.g., Di Prinzio et al. 2010; Chlaib et al. 2014; Antoine et al. 2015). GPR has been used in many applications in the last decades as it is a nondestructive and high-resolution shallow geophysical technique that can resolve various defects and structural and compositional changes. It is widely used for detecting animal burrows, which can be considered one of the main reasons for levee failures by piping phenomena (Di Prinzio et al. 2010). GPR was suggested as a standalone technique in investigating animal burrows (Di Prinzio et al. 2010). The affordability of GPR was also considered in discriminating voids from water-filled cavities or metallic objects (Chlaib et al. 2014; Samyn et al. 2014). A good matching was clear between the observed features and the interpreted anomalies. However, validation of results by field evidence, geotechnical data, or other geophysical techniques is crucial, as mentioned by Borgatti et al. (2017) and Sentenac et al. (2017). Another major issue affecting levee health is the occurrence of sections with more porous compositions or complex structures where seepage can develop, and GPR can also be applied in identifying these risky sections (Antoine et al. 2015; Busato et al. 2016).

The main objective of our study is to develop a set of tools to map and relatively easily assess the risk related to potential levee malfunction using a 40-km-long test site along the Lower Tisza River. This is because many researchers usually target the identification of certain types of defects, but there is yet no inventory of the type of defects that can be identified using GPR. However, in this research, we focus on the analysis of different types of defects, which are then categorized according to their potential risk and levee health. This required identifying and interpreting different types of anomalous features within the levee body, allocating sections affected by considerable height decrease over time, and verifying remotely sensed data through field observations of flood phenomena. The inventory of defects and the developed levee health evaluation method can be applied for future large-scale surveys along the Tisza River and other large alluvial rivers with artificial levees. Therefore, we present the novel idea of integrating different methods, such as GPR, Persistent Scatterer Synthetic Aperture Radar (PSI), and GPS, for easily evaluating levee health and verifying the outcomes from historical flood phenomena records.

2 Case study

The Tisza River (catchment area: 157,000 km²) in Central Europe drains the eastern half of the Pannonian Basin, where river systems have a long evolution history. The oldest fluvial deposits date back to the Late Miocene (Gábris and Nádor 2007). The courses of the rivers, including the Tisza, are influenced by several sinking grabens. One of the most active ones is the South Tisza Graben, where approximately 700-m-deep fluvial sediments

have accumulated (Ronai 1985). Until the Late Pleistocene, the subsidence of the graben was continuous but fluctuating (Kiss et al. 2014); during the Holocene, it terminated as Early Holocene floodplain forms were not buried by younger sediments (Kiss et al. 2012). However, in historical times, the subsidence became active again, mainly driven by natural gas, oil, and water extraction.

The analyzed artificial levee section (Fig. 1) of the Lower Tisza River (Hungary) is 40 km long and is located at the left bank of the river, from 12 to 50 Lkm (Lkm: levee kilometer).

In the late nineteenth century, catchment-scale engineering interventions began on the Tisza River to prevent floods' recurring inundation of vast areas. These works included the disconnection of the Tisza from its floodplains through the construction of artificial earth embankments or levees. The total length of the levee system along the Tisza is 2940 km. Because of interventions along the river (e.g., cut-offs) and on the catchment

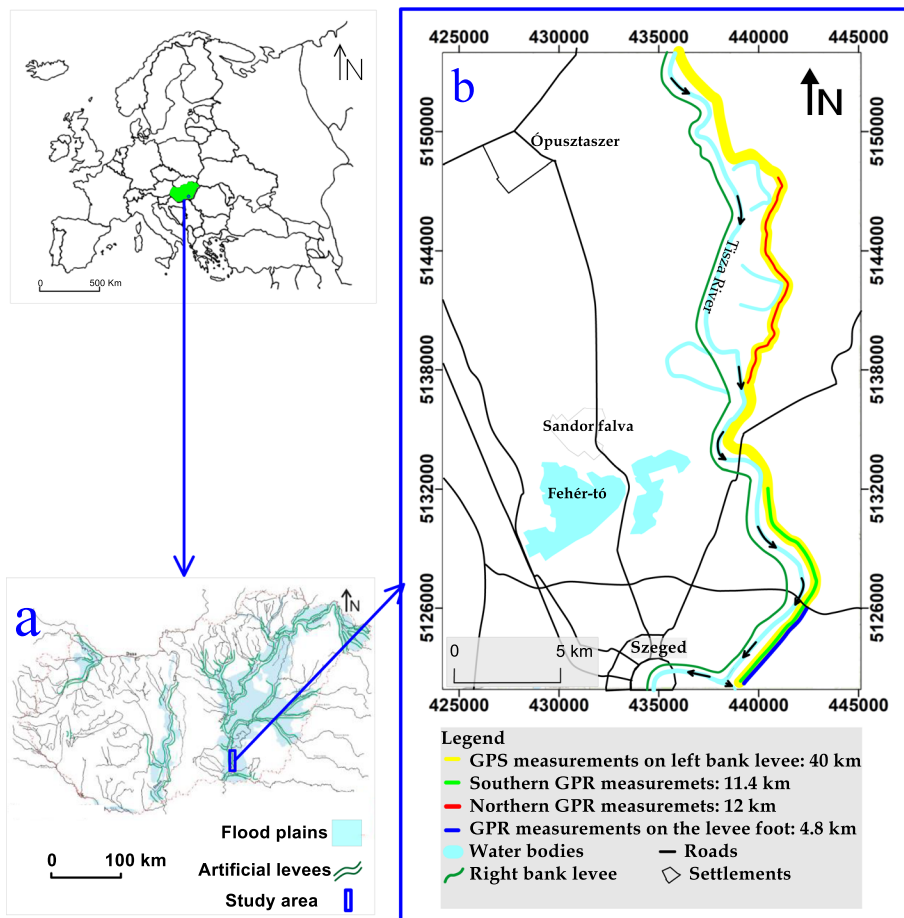


Fig. 1 a Location map with potential floodplains and artificial levees in Hungary (modified after OVF 2014) and b the study area showing the places of RTK-GPS measurements as a yellow line, southern GPR measurements on the levee crown as a green line, northern GPR measurements on the levee crown as a red line, and GPR measurements on the levee foot as a blue line

(e.g., forest clearance), the frequency of floods increased continuously over time. Therefore, the levees were heightened several times in the past 150 years, which resulted in an onion-like, complex structure with several layers (Fig. 2). Currently, their relative height ranges between 5 and 8 m (Kovács 1979; Nagy 2000). The precise structure and composition of the levees are only known along newly constructed sections, as works in the nineteenth century were scarcely documented. Moreover, because of the application of nearby materials, such compositions can be highly heterogeneous in vertical and horizontal terms. Consequently, mapping structural and compositional changes are crucial from the perspective of future flood management.

3 Methods and materials

3.1 Elevation measurements

The long-term height change of the investigated levee section was assessed by comparing archive leveling data with recent real-time kinematic GPS (RTK-GPS) measurements. GPS-based height changes, however, are hard to evaluate in terms of surface deformation as there can be several other factors in the millimeter to centimeter range affecting levee height besides geologically driven subsidence or uplift. Therefore, subsidence velocity was also estimated using PSI data.

GPS measurements were performed on the levee crown and levee foot at every 200 m between 12.5 and 42.0 Lkm using a TopCon Hyper Pro device in 2017 and 2018 (Fig. 3d). The 3D accuracy of the instrument was measured to be 2–3 cm. Concerning the levee crown, baseline elevation data were derived from differential leveling made by the Lower Tisza Directorate in 1976. Leveling data were referenced to the national benchmark system at the time, which was later renewed and incorporated into the National GPS Network. Still, there is a spatially variable height difference between the two systems; at the study

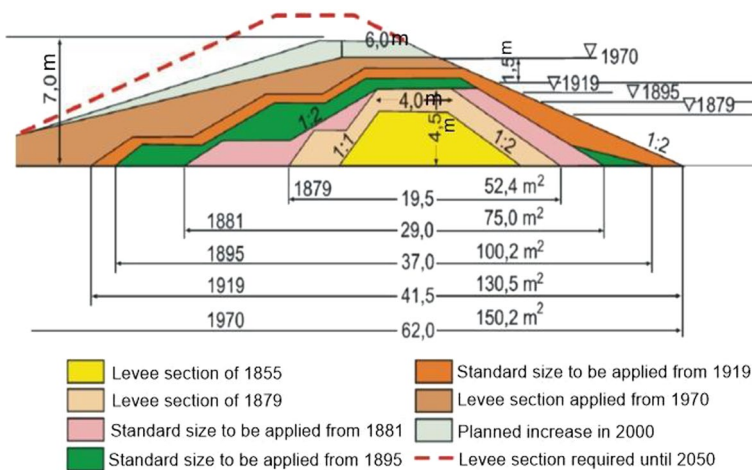


Fig. 2 Typical structure of levees along the Tisza River. Heights are given in meters (adapted from Schweitzer 2002)



Fig. 3 **a** Tensile cracks on the levee crown, **b** GPR survey using SIR3000 attached to a 200-MHz shielded antenna on the levee crown, **c** GPR survey on the levee foot, and **d** location of GPS points measured on the levee crown and levee foot

site, this difference is estimated to be 6 to 7 cm (Hivatkozás). Consequently, we corrected the leveling data by -7 cm to obtain more realistic height change values.

Along the levee foot, our GPS measurements were compared with the data of an earlier GPS survey, made again by the directorate in 2003. The points of the 2003 survey were staked out at least with a 5-cm horizontal precision, and the height was measured again. In this case, no additional corrections were made as both surveys used the same reference system.

Acknowledging the above-mentioned uncertainties, measurements were complemented by space-based PSI data to verify the height change derived from geodetic data. PSI analysis was based on 70 ERS-1, ERS-2, and Envisat Single Look Complex data of the European Space Agency acquired between 1992 and 2010. For every 500-m section between 12.5 and 39.0 Lkm, average vertical velocity values were calculated from those

PSI point targets located on and around the levee within a 1500-m buffer zone. The width of the buffer zone decreased to 300 m near the city of Szeged because of the greater point density.

3.2 GPR data acquisition and processing

GPR is a fast, non-invasive, and high-resolution electromagnetic technique transmitting high-frequency electromagnetic pulses, which are partly attenuated but also reflected from the interface of layers or objects with different dielectric properties. The greater the dielectric permittivity contrast, the higher the experienced reflectance. The penetration depth of GPR is directly related to the frequency and wavelength of the transmitted electromagnetic pulses. It is related to the type and state of the soil as well. The maximum penetration depth equals 20 wavelengths (Daniels 2004); however, in most cases, depending on the electromagnetic properties of sediments, the depth is considerably less than this (Utsi 2017).

The GPR survey was conducted using a SIR 3000 control unit (Geophysical Survey Systems Inc.) attached to a 200-MHz center frequency antenna in the survey wheel mode (Fig. 3). We recorded 1024 samples per scan (16 bits per sample) to achieve a high vertical resolution. The scanning rate was set to 64 scans per second. Meanwhile, data were acquired at 60 scans per meter to achieve a high horizontal resolution of the collection. The time range window was set to 170 ns, the gain and the position of the first positive peak were set automatically, and the dielectric constant was kept at 16 throughout the measurements, depending on the conductive nature of the levee materials.

The GPR survey was performed in two sections (southern zone: 12.6–23.9 Lkm; northern zone: 31.2–43.1 Lkm), separated by a 7-km-long asphalted levee section. Measurements were performed on the levee crown and at some places at the levee foot (Fig. 3b, c). The total number of GPR profiles was 282. Each GPR profile had a length of 100 m. The profiles were successive; that is, the endpoint of one profile is the starting point of another profile. Concerning the southern zone, 162 GPR profiles were measured, of which 114 were made on the levee crown and 48 on the levee foot. In the northern zone, 120 GPR profiles were taken, each on the levee crown, as shown in Fig. 1.

As no filters were applied during data acquisition, the signals contained different types of unwanted signals that had to be eliminated as low-frequency noise, high-frequency monochromatic unwanted signals, spurious noise, and flat-lying noise (horizontal bands of noise) originating from antenna ringing and any other reflections arriving from above the ground (e.g., reflections from nearby vehicles, buildings, fences, power lines, and trees). We used the software REFLEXW 8 (Sandmeier 2016) and RADAN 6.6.2.1 (GSSI 2010) to improve the signal-to-noise ratio. The first step of processing was time zero (T_z) removal to compensate for the delay in the first arrivals. The filter parameter move time determined the time value for each trace that must be shifted. In the data, the move time parameter was set to -14 ns.

The second step was a background removal filter to remove the horizontal banding caused by the GPR and any other reflections from above the ground (e.g., reflections from nearby vehicles, buildings, fences, power lines, and trees). It also suppressed horizontally coherent energy. Because this filter removes the direct coupling pulse, it was applied after time zero correction. The filter subtracts an averaged trace (trace

range), which is built up from the chosen time/distance range of the actual section. The start time was set to 0 ns, and the end time was set to 156 ns.

The third step was a 1D filter for the subtraction of the mean (Dewow) to eliminate the drift of traces from the mean over time and to remove the low-frequency part (dewow) from the received signal (Sandmeier 2016). The filter acted on each trace independently, and a mean running value was calculated for each value of each trace. Then, this running mean was subtracted from the central point.

The fourth step was a 1D bandpass frequency filter that removed additional high-frequency monochromatic signals but retained low-frequency noise not corresponding to the frequency range of the GPR (Sandmeier 2016). It was applied to each trace. The lower cut-off was set to 10, the lower plateau was set to 85, the upper plateau was set to 185, and the upper cut-off was set to 300.

The fifth step was a 2D filter running average. This filter emphasized horizontally coherent energy to make targets clearer and to reduce any associated spurious noise (Utsi 2017). The running average was performed over several traces to suppress trace-dependent noise. The average traces used here were 7.

In the sixth step, the gain was set manually in the y -direction as each signal passed into the ground; some parts were lost into the environment (attenuated), and others reflected the receiver so that each with increasing depth signal diminishes (Utsi 2017). It allowed us to interactively define a digitized gain curve in the y -direction (normally time axis) and apply this gain curve to the data.

After processing, the GPR profiles were analyzed to identify interfaces and record different types of anomalies. Anomalies were then categorized and evaluated in terms of flood-risk. The spatial distribution of the different categories was analyzed concerning other parameters referring to levee health. Besides mapping structural differences and defects, changes in levee composition were also assessed, mostly by investigating the attenuation of signals. Differences in attenuation were expressed by determining effective penetration depths at a fixed dielectric constant ($\epsilon = 16$). Penetration depth was calculated using the automated Max Depth function of the software RADAN, analyzing the noise and signal loss from trace to trace. As the surveys along the studied levee sections were made on consecutive days, the environmental conditions, especially moisture content, were uniform, and we assumed a direct relationship between penetration depth and the grain size/porosity of the sediments building up the levee body.

3.3 Methodology of levee health evaluation

The risk potential at every kilometer of the investigated levee sections was assessed by combining the different data we obtained. The analysis was conducted by calculating (1) the mean elevation decrease, (2) the mean penetration depth, and (3) the mean number of anomalies per 1 km for the entire investigated area. These values were compared with those calculated for 1-km sections (Fig. 4). At each 1-km section, the values of the above three parameters were compared with the mean for the entire section. If the 1-km value was below the section mean, it received a score of 1, referring to a lower level of levee health (LLLH) than the average. In contrast, if the 1-km value was higher than the section means, it received a score of 2, referring to a higher level of levee health (HLLH) than average. Subsequently, scores of levee health levels were added up; for each 1-km section, a potential level of levee health value was assigned, with scores of 3 and 6 meaning low and very high levels of levee health potential, respectively (Fig. 4).

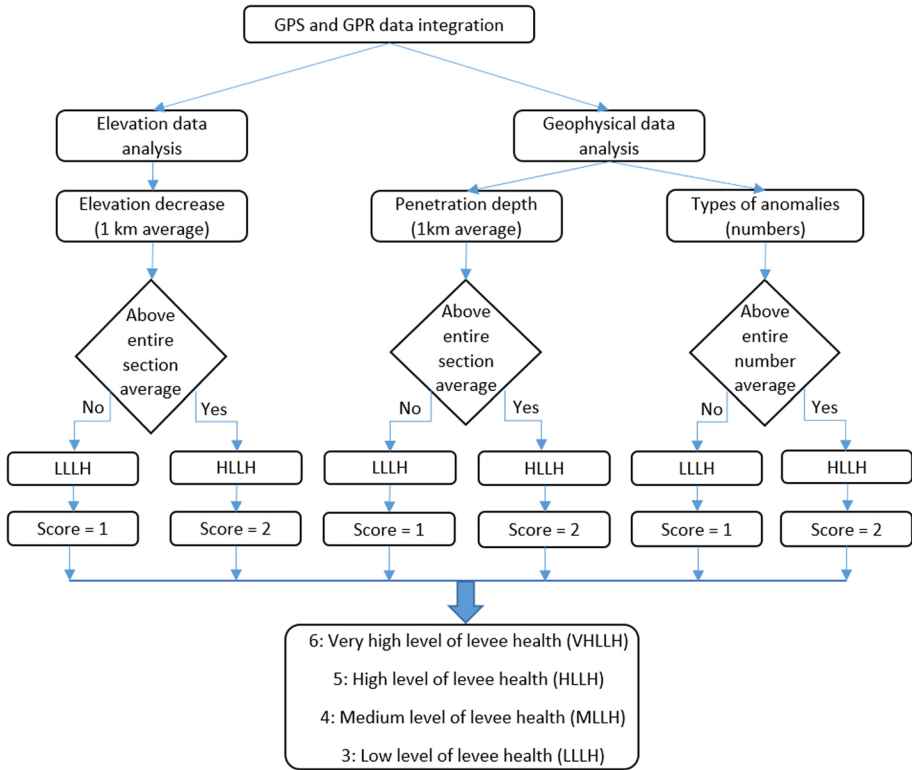


Fig. 4 Diagram for calculating health along the investigated levee sections

3.4 Inventory of historical flood phenomena

High flood levels and extensive flooding can lead to the gradual soaking of the levee body, which can decrease the flood resistance capacity of the earthwork and, in extreme situations, lead to the failure of the structure. Therefore, identifying and recording different flood phenomena during floods are major tools in the hand of levee guards to assess the levees’ status and locate weak sections. From the 50-year-long record of the Lower Tisza Water Directorate, six types of flood phenomena have been identified along

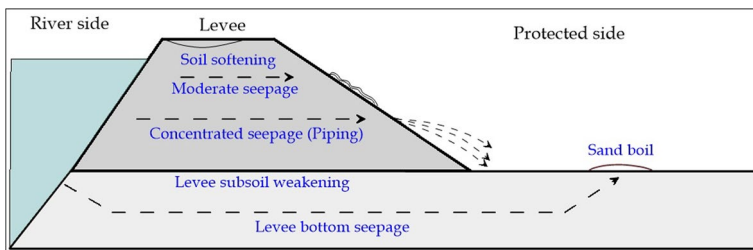


Fig. 5 Six types of flood phenomena identified by the Lower Tisza Water Directorate along the investigated levee section

the studied levee section: soil softening, moderate seepage, concentrated seepage (piping), levee subsoil weakening, levee bottom seepage, and sand boil (Fig. 5). These have been recorded since 1970 along the investigated levee section. Since then, 11 significant floods have caused flood phenomena. From an overall review of recordings, seepage and piping were identified as the most frequent phenomena in the investigated area. These affected the upper part of the levee body, mostly within the estimated range of GPR penetration depth. Following the extreme floods in 1970 and 2000, the investigated levee section was reinforced at several critical sites, and recordings of the subsequent 2006 and 2010 floods were chosen to determine the spatial distribution of flood phenomena and their relationship with geophysical data. In the past 20 years, the largest and most damaging flood was in 2010 (Borsos and Sendzimir 2018).

Flood phenomena were recorded on digital blueprints showing their actual position along a scale representing the levee. If their spatial frequency was high at certain sections, they were not marked individually, but intervals of occurrence were recorded. Graphical data were converted into an excel sheet: each 100-m section was evaluated as either affected by flood phenomena (score 1) or not (score 0). The scores from both investigated years were summed for each levee kilometer and plotted against the horizontal distance along the investigated levee section. The frequency diagram of seepage and piping phenomena was compared with the spatial frequency of anomalies identified using GPR profiles.

4 Results

4.1 Elevation change

In general, the elevation values were lower in 2017 than in 1976 (Fig. 5). The corrected mean height of the levee crown in 1976 was 85.26 m asl. In 2017, it was 85.21 m asl. The calculated 5-cm decrease in levee crown elevation does not seem significant at first glance. However, it must be underlined that at some sections, a slight elevation increase could be identified concerning pavement construction and repeated asphaltting during the study period (Fig. 6). If these sections are disregarded, the height difference is -8 cm (1976: 85.23 m asl.; 2017: 85.15 m asl), which is significantly higher than the expected

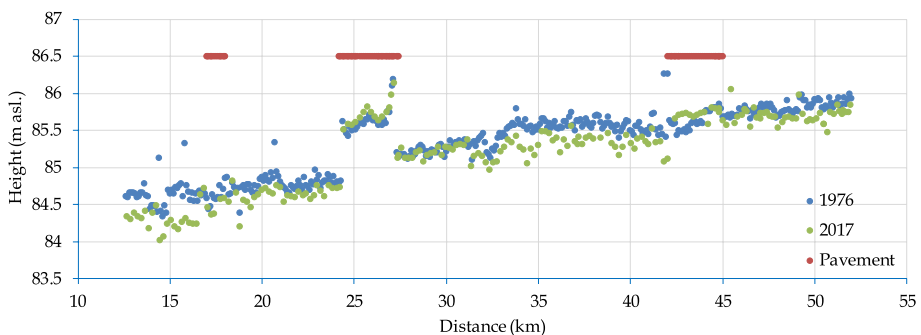


Fig. 6 Elevation data for the levee crown in 1976 (blue points) and 2017 (green points). Red lines mark sections where the levee crown is paved

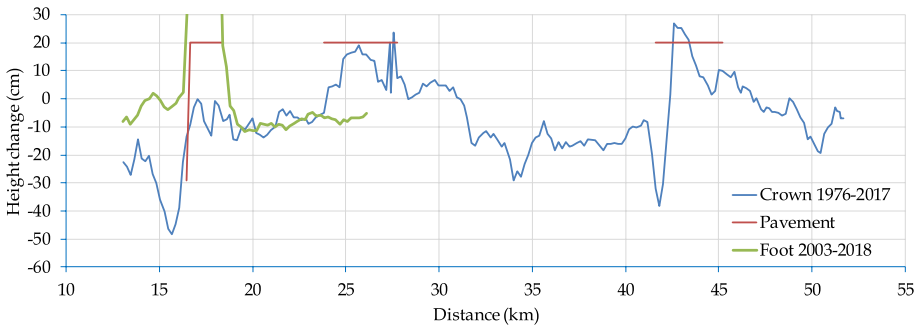


Fig. 7 Elevation change of the levee crown (blue line) and levee foot (green line) along the investigated sections using a 1-km moving average

measurement errors. Therefore, the annual subsidence rate for these sections is 1.3 mm/year.

For a more detailed investigation, the spatial variations of changes and elevation differences were also evaluated by applying a moving average analysis (1-km window at 200-m steps) (Fig. 7). Even in terms of unpaved sections, the height change was not uniform; that is, some parts were affected more by elevation decreases, such as the levee section between 32 and 41 km (−16 cm on average) or between 13 and 17 km (−29 cm on average). Such spatial differences imply that elevation decrease cannot simply be explained by compaction and mass-related subsidence, which should affect the entire section similarly. Instead, there can be other forces leading to non-uniform subsidence.

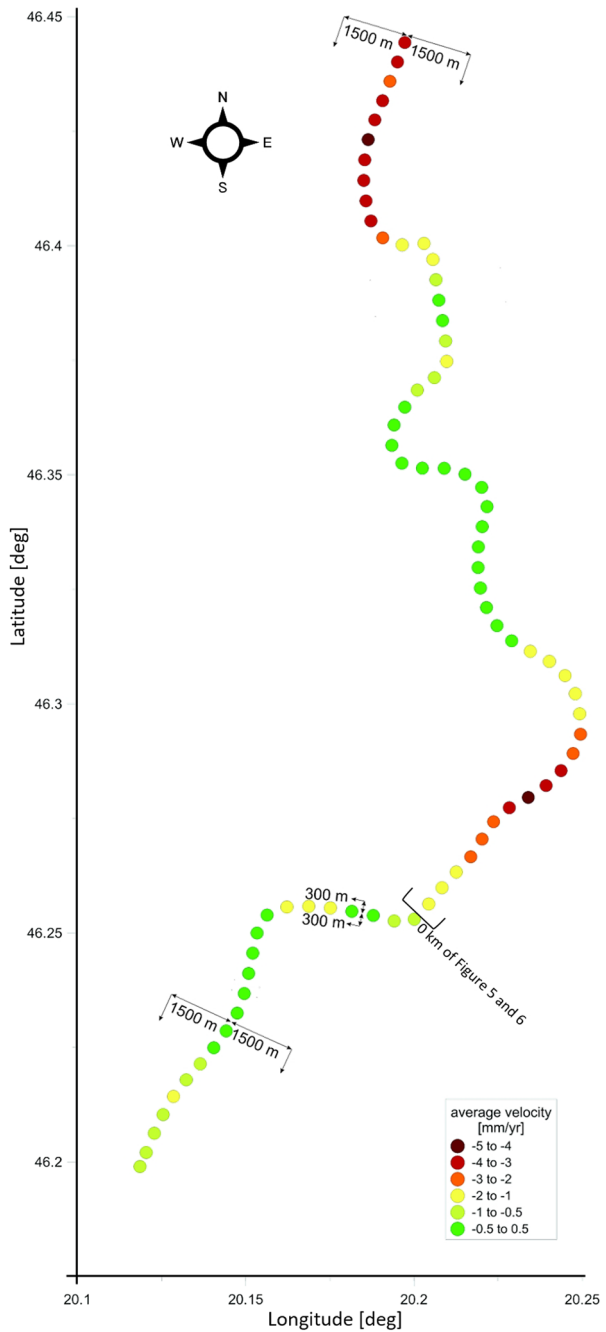
Concerning the levee foot, elevation values, as in the case of the levee crown, were lower in 2018 than in 2003 in the investigated section. In comparing the two datasets, points that showed extreme elevation increases were excluded. These were unambiguously related to the reinforcement of the levee foot upon the construction of a highway bridge over the river between 2009 and 2011.

Consequently, the mean height of the levee foot was 78.31 m asl in 2003 and 78.25 m asl in 2018. This shows a general 6-cm decrease. The annual rate of height loss for the 15-year-long period was then 3.7 mm/year, corresponding remarkably well to the annual height decrease of the levee crown on the same levee section between 1976 and 2017, which was also 3.7 mm/year.

Although the levee foot height was also affected by engineering interventions, such as reinforcements, it exhibited a more uniform change, partly due to the shorter period of investigation and the presence of fewer factors affecting elevation conditions. Although the spatial patterns of the levee crown and levee foot elevation decrease were not identical, the general trends on unpaved sections, such as between 13 and 17 km and between 19 and 24 km (Fig. 7), were the same, meaning that the levee crown and foot moved together. Thus, there should be a subsidence process affecting the entire levee body.

The spatially uneven subsidence in the area was also reinforced by the PSI data, representing the levee and its environs. In the investigated 18-year period (1992–2010), surface deformation velocities ranged between +0.5 and −5.0 mm/year (Fig. 8). Thus, the average subsidence rate along the investigated Sect. (12.5–39.0 Lkm) was

Fig. 8 Average deformation velocities between 1992 and 2010, calculated from PSI data falling within a 1500-m buffer of the levee. Data were averaged for every 500-m section



1.9 mm/year. This value is very close to the rate calculated using leveling and GPS data (1.3 mm/year), though a longer section was assessed in the latter case. Suppose only parts measured by both methods were evaluated, excluding paved sections. In

that case, the traditional estimate of subsidence is higher (4.2 mm/year) than the PSI-derived values (2.6 mm/year). The difference may have arisen from the different periods of analyses. Thus, vertical velocities may have changed over time. Still, the results of the two methods verify each other well. If any of the obtained data are considered significant, subsidence has affected the investigated levee section over the past decades, and the spatial distribution of this process is quite uneven. Consequently, large-scale anthropogenic activity might explain deformation and subsidence anomalies (Grenerczy et al. 2021), a potential source of which can be intensive oil and natural gas extraction in the area from the 1970s (Kiss et al. 2021).







4.2 Identification of GPR anomalies

After processing the GPR profiles, six types of anomalies were identified, each affecting flood-risk differently by modifying the levee structure. As shown in Table 1, the anomalies picked up from all the affected sections were categorized and evaluated in terms of flood hazard. The number of GPR profiles affected by each of these anomalies was counted.

The different types of anomalies are explained in detail as follows:

1. *Tensile cracks* cracks form when the shear stress exceeds the shear strength of soils (Wei et al. 2020; Lu et al. 2007). The most frequent anomalies detected in GPR profiles were tensile cracks on the levee crown, as shown in Fig. 3a. They appear on the GPR profiles as vertical lines with a dielectric permittivity different from that of the surrounding levee materials. GPR profile No. 62 (Fig. 9a) shows an example of this anomaly type. Tensile cracks might close during wet periods and open again during dry periods, which damages the levee body in the long-term. Hundreds of cracks and nearly 30% of the investigated profiles were affected.
2. *Remarkable changes in dielectric permittivity* According to Utsi (2017), this phenomenon can be described by the increased (signal band lengthening) or decreased (signal band shortening) water content of levee materials. In several profiles, a remarkable and sudden change in dielectric permittivity was estimated qualitatively in the second layer of the levee structure (Fig. 9b). In Fig. 9b, high and low dielectric permittivity, therefore, may also refer to changes in the wetness of the levee material. However, these sudden changes are more probably related to increased clay (signal band lengthening) or silt/sand (signal band shortening) as all measurements were made during a long drought period, during which the groundwater level was estimated to be around 10 m below the survey depth. Although attenuation may also affect the banding pattern, the occurrence of highly different band lengths in the same profile indicates the greater importance of differences in levee material. This type of anomaly can cause seepage and mass failure. It was observed in many GPR profiles, and approximately 20% of the profiles were affected.
3. *Animal burrows* Burrows are tunnels or holes that an animal digs for habitation (a place to live) or as a temporary refuge (a place of protection) (Website 1). Air-filled animal burrows are characterized by a low dielectric constant (ϵ_r for air equals 1), so the reflected signal from its boundary changes its polarity relative to the incident signal (Smith and Scullion 1993; Chen and Wimsatt 2010). In the radar scan across an empty animal burrow, a positive peak appears depending on its size. They are frequently eroded, especially in the levee structure (Seed et al. 2006; Wiscomb and Messmer 2010). This anomaly is one of the most common problems that form piping in levee

Table 1 Different anomalies identified from the interpretation of 2D-GPR profiles and their evaluation in terms of flood-risk

No.	Legend	Name	Evaluation in terms of flood hazard	Number of GPR profiles affected
1		Tensile cracks	Enables piping, leading to levee breach or mass failure Cracks might close when the levee gets wet	87
2		Remarkable changes in dielectric permittivity	Enables seepage, leading to mass failure	70
3		Animal burrows	Enables piping, leading to levee breach or mass failure	33
4		Layer deformation	Results in height decrease, overtopping	6
5		Paleo river channel	Enables seepage below the levee, leading to water upwelling and the development of sand boils	5
6		Sudden change in stratification (dipping layers)	Enables contour line seepage, leading to mass failure	4

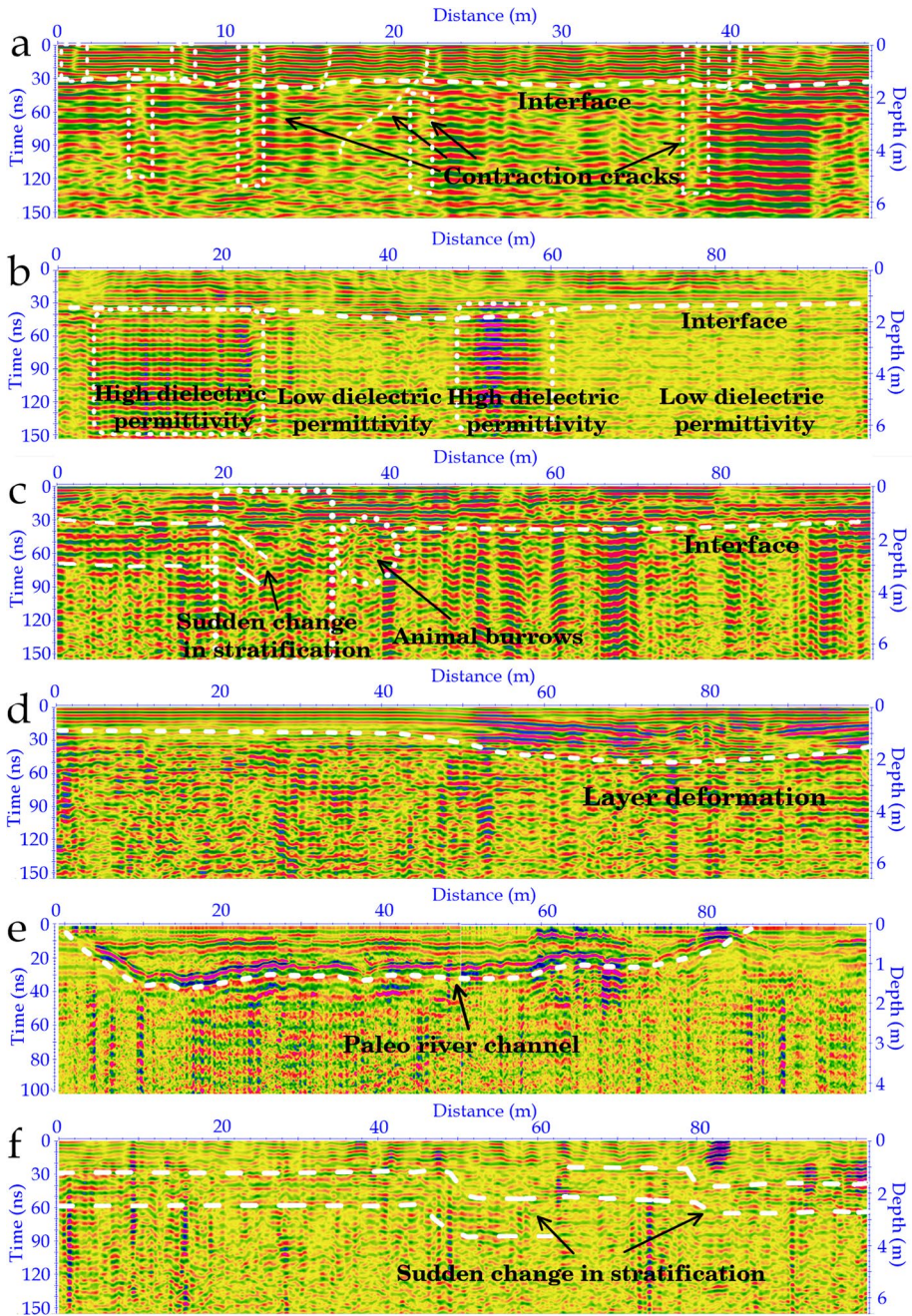


Fig. 9 Representative profiles for the identified GPR anomaly types: **a** tensile cracks (profile 62, southern zone), **b** remarkable changes in dielectric permittivity (profile 24, southern zone), **c** animal burrows and sudden changes in stratification (profile 54, southern zone), **d** layer deformation (profile 18, southern zone), **e** paleo river channel at the levee foot (profile 42, southern zone), and **f** sudden change in stratification (profile 60, northern zone)

- structures. The piping phenomenon leads to approximately half of the world's dam failures (Richards and Reddy 2010). Approximately 10% of the profiles were affected by these features. Figure 9c shows an example of anomalies resulting from animal burrows.
4. *Layer deformation* Minor deformations regarding performance limit states are defined by non-discernible shear zones (max deviatoric strain less than 1%) and low gradients (i.e., $i < 1$) throughout the embankment dam and foundation (Khalilzad and Gabr 2011; Khalilzad et al. 2014, 2015). Deformation in the levee layers can appear in GPR cross-sections measured on the levee crown as a distinguished change in the dielectric permittivity in the top layer ~ 1 to 2 m thick, with a strong reflectivity characterizing the subsidence part. This anomaly negatively affects the levee height as it causes a height decrease; thus, the levee needs to be heightened over time. Figure 9d illustrates an example of layer deformation. Six GPR profiles showed signs of this phenomenon.
 5. *Paleo river channel* Palaeochannels are remnants of rivers or stream channels that flowed in the past and have been filled or buried by younger fluvial sediments. Paleo river channels have been investigated using GPR (e.g., Vandenberghe and van Overmeeren 1999; Skelly et al. 2003; Slowik 2012). The strong reflector of this anomaly on a GPR cross-section shows a concave shape representing the river's outer banks, and the weak reflectors inside represent the currently filled younger sediments. Paleo river channels are considered one of the important causes of levee failure as they allow seepage below the levee and can increase flood-risk. The consequences of this phenomenon can be noticed in the protected side of the levee in the form of water upwelling. Paleo river channels can be observed only in GPR profiles measured on the levee foot. Figure 9e illustrates an example of a paleo river channel. In total, five GPR profiles were affected.
 6. *Sudden change in stratification* This phenomenon is defined as a sudden slope in the horizontal levee layers, which might refer to considerable changes in the structure of the levee. In other words, the construction might have not followed a consistent design 150 years ago. It appears on the GPR profiles as an abrupt decline in the horizontal reflectors of the levee layers. This anomaly might increase seepage during floods and may constitute areas of mass failures. In this research, a qualitative method of anomaly assessment was used. Sudden stratification changes were observed in four profiles (Fig. 9c, f).

4.3 Spatial distribution of GPR anomalies and penetration depth

Penetration depth, like changes in dielectric permittivity and antenna frequency, is mostly determined by the state of the levee material. According to the inverse relationship between the velocity of GPR signals and the relative dielectric permittivity of different materials ($v = ct/\sqrt{\epsilon r}$; Annan 1996), the higher penetration depth of the signals meant that this part of the levee is composed of materials that permit electromagnetic waves to pass with higher speed than those through other parts of the levee. The lower relative dielectric values explain these parts with higher penetration depths. The spatial penetration depth variation refers to levee material changes, with lower depths indicating higher clay content and greater depths indicating higher silt or sand content (Fig. 11b). The penetration depth of the Southern GPR survey zone ranged from 3.3 to 4.5 m, with an average of 3.73 m. Although values fluctuated, it seems clear that there are three separable zones within this section with increased penetration depth. These zones are between 14.4 and 15 km, 17.5 and 18.8 km, and 21.5 and 23 km (Fig. 11b).

Meanwhile, the penetration depth at the northern measurement zone ranged from 3.2 to 4 m, with an average of 3.4 m. In contrast to the southern measurement zone, fluctuations herein were smaller, and only one section exhibited an increased penetration depth between 34 and 35 km. The northern zone appears to be more stable and homogeneous in composition. In the case of the penetration depth analysis for the profiles measured on the levee foot, the values ranged between 3.5 and 4.5 m, with an average of 3.9 m marked as a red line in Fig. 11b. The outcomes of the anomalies from the 2D-GPR measurement sections are represented in one chart (Fig. 11c).

From the comparison of the results of the penetration depth of the GPR signals with the outcomes of the anomalies for both the southern and northern measurements of the levee, the inhomogeneity and frequency of GPR anomalies of the southern levee zone are the two main reasons behind this noticeable fluctuation of the GPR penetration depth signals. Meanwhile, in the case of the northern zone, the penetration depth results show stability, which may be due to the homogeneous nature of the materials and the fewer anomalies detected from the GPR profiles in this zone (Figs. 11b and 7).

4.4 Verification of GPR results using flood phenomena records

The GPR results were compared with 2006 and 2010 piping and moderate seepage recordings along the studied levee section (Fig. 10). For the spatial comparison, the frequency of all GPR anomalies and anomalies referring to a remarkable change in dielectric permittivity was applied. The latter parameter was chosen because of two reasons: (1) it was the second most abundant anomaly with enough recordings to make a spatial plot and (2) this type of anomaly was mostly experienced in the second layer of the levee structure, at a height where piping and moderate seepage usually appear. Thus, tensile cracks and animal burrows were not considered in detail as these affect only the top part of the levee.

Although the spatial patterns of km-based data of anomalies and flood phenomena do not match completely, the general difference between the two investigated zones is obvious. In the case of the southern and northern zones of the investigated levee section, 148 and 42 anomalies were detected, respectively. Out of these, 51 and 18 were classified under sudden changes in dielectric permittivity. Meanwhile, the numbers of 100-m sections affected by piping or moderate seepage regarding the two zones were 26 and 11, respectively. If the summed recordings of a zone are expressed as the percentage of total recordings, then the relationship is even more obvious. The proportionate values of piping and moderate seepage were 70% and 30% in the southern and northern zones, respectively. Similar values were obtained when remarkable changes in dielectric permittivity were considered (74% vs. 26%), and a somewhat different but comparable distribution was experienced when each type of anomaly was considered (78% vs. 22%).

Although the pattern of the recordings is not entirely the same, the frequency of flood phenomena cannot be directly predicted from GPR anomalies. However, if longer sections are investigated, the trend is obvious, and GPR can be applied to assess the potential for seepage and piping occurrences.

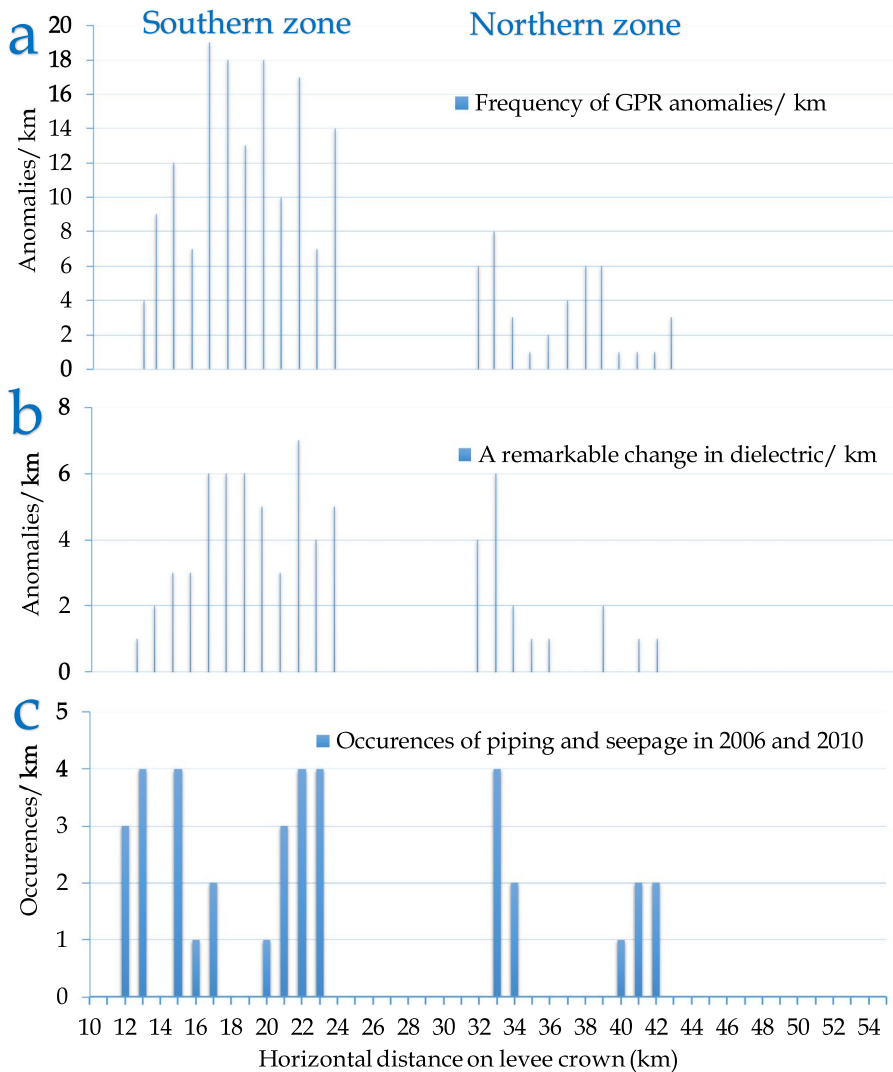


Fig. 10 **a** Spatial frequency of anomalies identified from GPR profiles measured on the levee crown (each 1-km section), **b** special frequency of a remarkable change in dielectric for each 1-km section, and **c** occurrence of concentrated seepage (piping phenomenon) for each 1-km section during two flood periods in 2006 and 2010

5 Discussion

In our study, similar defects were detected through the combined use of GPR and GPS, as in the case of the study of Tanajewski and Bakula (2016), but in a 40-km section of the investigated levee. PSI measurement offered a fast way of detecting surface deformation along the investigated levee, especially when GPS supports it and leveling data. However, GPR data can also provide better insights into the levels of healthy sections of the levee.

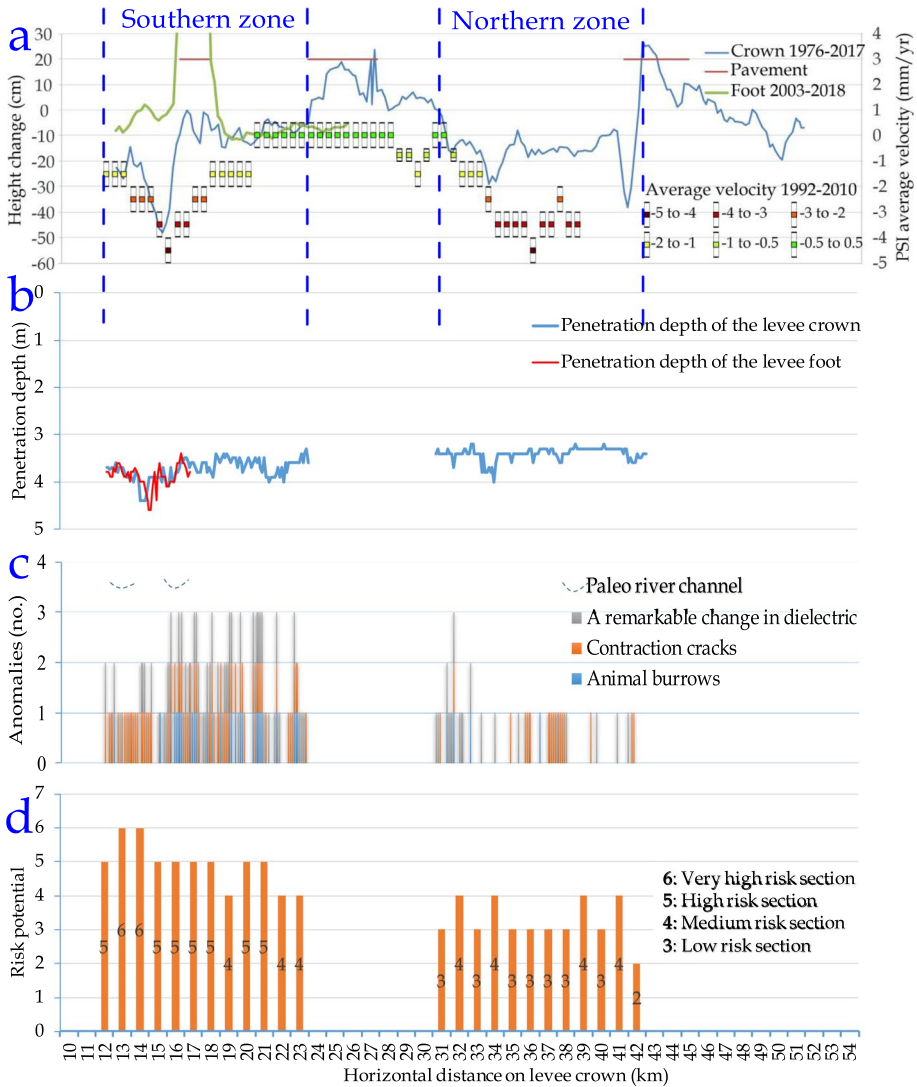


Fig. 11 Spatial distribution of parameters influencing flood-risk related to the levee in the study area. **a** Moving average of elevation change between 1976 and 2017, **b** penetration depth of GPR signals, **c** types and spatial frequency of anomalies identified on the GPR profiles taken on the levee crown, and **d** risk evaluation for each 1-km section of the levee

Most researchers studied and analyzed animal burrows for assessing levee health (Masannat 1980; Mazzini and Simoni 2008; Di Prinzio et al. 2010; Chlaib et al. 2014; Borgatti et al. 2017). However, in this study, the flood phenomena affecting levee health were related to other types of defects aside from animal burrows. Thus, different types of defects must be combined and assessed in parallel to establish a relationship between the flood phenomena and different types of anomalies as one type of defect is not enough to provide a good image of the current status of the investigated levee. Among various

types of anomalies, tensile voids and cracks were identified in our study, but they mostly get closed by the wetting of the levee body during floods. However, the largest ones may remain open (Szűcs et al. 2019), which means that their presence can increase the risk of damage as leakage through cracks usually leads to piping, which is the main cause of levee failure events (Huang et al. 2014; Cleary et al. 2015; Antoine et al. 2015).

By comparing the leakage areas in the levees detected using GPR in the earth embankment from Antoine et al. (2015) with our data, we could notice that such an anomaly was not discovered in our investigated levee sections. One type of burrow classified by Chlaib et al. (2014), which includes small air-filled burrows, can be detected using the signal polarity and the dielectric contrast with the surrounding levee materials in the riverside edge and is similar to animal burrows detected in our studied levee section. Meanwhile, paleo river channels detected in several GPR profiles measured on the levee foot match with the results of many previous studies (e.g., Vandenberghe and van Overmeeren 1999; Skelly et al. 2003; Słowik 2012; Ritambhara et al. 2021), with a special reflector characteristic explaining the old banks and the younger sediments that filled these channels.

Surface deformation was detected in several GPR profiles measured on the levee crown. In Kiss et al. (2021), surface deformation related to subsidence or uplift is one of the main factors causing height decrease in artificial levees. Also, the southern half of the study area is located above the Algyő Oil and Gas Field (~50 km²), which has operated with 1011 wells and drained oil and gas from depths of 1723–2500 m since 1970 (Konx et al. 2022). According to Joó (1996), the subsidence related to this mining activity is 3.6–4.1 mm/year. As most of the extracted reserves are under the channel and floodplain of the Tisza and Maros Rivers, the subsidence can dramatically change the elevation and stability of the artificial levees.

The combined use of ERT and GPR and their validation by borehole data, as done by Sheishah et al. (2022) on one section of the Tisza levee, could reveal the levee composition, which consists of fine and medium silt units, and one reason for such fluctuation in the penetration depth of the GPR signals (especially in the southern levee zone) could be explained. The combined results of the leveling data from 1976 and GPS data measured in 2017 were spatially fitted to GPR penetration depth data and the distribution of anomalies detected on the levee crown.

Going from north to south, an increasing trend can be seen in the levels of levee health scores (Fig. 11). LLLH sections predominated in most of the northern zone, except for four 1-km sections with a medium level of levee health (MLLH) (at 42, 40, 35, and 33 Lkm). In contrast to the northern zone, mostly HLLH sections can be identified in the southern zone, and even very high levels of levee health sections occur (at 16 and 15 Lkm), whereas MLLH sections are restricted only to the first part of this zone at 24 and 23 Lkm. Accordingly, the mean levels of levee health score are 5.0 in the southern zone and 3.4 in the northern zone, indicating the overall worse condition of the previous section. Consequently, the southern levee zone can be considered more prone to flood phenomena and failure during floods.

6 Conclusions

On the basis of the geophysical surveys conducted on the Tisza levee section, we conclude that the combined use of GPS, PSI, and GPR with data validation collected from flood phenomena recordings is an effective approach for examining the levee conditions in terms of flood-risk and flood resistance capacity. From elevation and surface deformation velocity measurements, we observed a considerable height decrease along the surveyed levee crown and levee foot between 1976 and 2017. As different datasets for different periods on different parts of the levee point in the same direction, the role of subsidence as a matter of surface deformation seems reinforced. Considering PSI data, regional surface deformation is evidently a very important factor behind elevation changes along the levee. As it affects the absolute height of the levee locally, it is also a significant issue in terms of flood-risk. In most GPR cross-sections, the penetration depth of radar signals was limited, and anomalies could be identified up to 3 to 4 m. Following the categorization of anomalies, the investigated sections could be evaluated in terms of flood-risk. Remarkable changes in dielectric permittivity and tensile cracks represented the most common anomalies among all other identified defects. The spatial change in the heterogeneity of the investigated levee was also clearly marked by the variations experienced in penetration depth determined by the dielectric properties of the levee material. Thus, according to the GPR data, the health of the southern zone is much worse than that of the northern zone.

Regarding flood phenomena recordings since 1970, we found that among different types of flood phenomena, the spatial distribution of piping and moderate seepage can be compared with that for the GPR data as these affect the upper part of the levee body and are mostly within the experienced GPR penetration depth. Besides, these were the most abundant flood phenomena in flood years along the investigated levee section. We found that the frequency and spatial distribution of GPR anomalies corresponded well to flood phenomena; thus, using GPR surveys, the occurrence of piping and seepage during floods can be predicted. By integrating different types of results, high-, medium-, and low-flood-risk sections could be identified from the perspective of the condition of the levee. Generally, the southern zone received a much higher risk score than the northern zone, implying that the risk of failure during floods is considerably greater here. This information is very important for the maintenance of the levee and can also aid the planning of interventions during flood situations. Overall, our investigation proved to be adequate for evaluating levee health and can be extended to longer sections along the Tisza River and other rivers.

Acknowledgements We would like to acknowledge Sándor Kovács for his contribution during GPR data acquisition, and Gergő Gál for his help during GPS data collection. We also thank the support of Geo-Sentinel Ltd. under a European Space Agency (ESA) project No. 4000119892/17/I-NB. Additional support for GPR measurements was provided by Roden Ltd. under project 2018-1.1.2-KFI-2018-00029, funded by the National Research, Development and Innovation Fund, Hungary.

Funding Open access funding provided by University of Szeged.

Declarations

Conflict of interest The authors declare that they have no known competing financial interests or personal relationships that could have appeared to influence the work reported in this paper.

Open Access This article is licensed under a Creative Commons Attribution 4.0 International License, which permits use, sharing, adaptation, distribution and reproduction in any medium or format, as long as you give appropriate credit to the original author(s) and the source, provide a link to the Creative Commons licence,

and indicate if changes were made. The images or other third party material in this article are included in the article's Creative Commons licence, unless indicated otherwise in a credit line to the material. If material is not included in the article's Creative Commons licence and your intended use is not permitted by statutory regulation or exceeds the permitted use, you will need to obtain permission directly from the copyright holder. To view a copy of this licence, visit <http://creativecommons.org/licenses/by/4.0/>.

References

- Annan AP (1996) Transmission dispersion and GPR. *JEEG*. <https://doi.org/10.4133/JEEG1.B.125>
- Antoine R, Fauchard C, Fargier Y, Durand E (2015) Detection of leakage areas in an earth embankment from GPR measurements and permeability logging. *Int J Geophys*. <https://doi.org/10.1155/2015/610172>
- Borgatti L, Forte E, Mocnik A, Zambrini R, Cervi F, Martinucci D, Zamariolo A (2017) Detection and characterization of animal burrows within river embankments utilizing coupled remote sensing and geophysical techniques: Lessons from River Panaro (northern Italy). *Eng Geol* 226(March):277–289. <https://doi.org/10.1016/j.enggeo.2017.06.017>
- Borsos B, Sendzimir J (2018) The Tisza River: managing a lowland river in the Carpathian Basin. In: Schmutz S, Sendzimir J (eds) *Riverine ecosystem management*. Aquatic ecology series, vol 8. Springer, Cham, pp 541–560. https://doi.org/10.1007/978-3-319-73250-3_28
- Busato L, Boaga J, Peruzzo L, Himi M, Cola S, Bersan S, Cassiani G (2016) Combined geophysical surveys for the characterization of a reconstructed river embankment. *Eng Geol* 211:74–84. <https://doi.org/10.1016/j.enggeo.2016.06.023>
- Chen DH, Wimsatt A (2010) Inspection and condition assessment using ground penetrating radar. *J Geotech Geoenviron Eng* 136(1):207–214. [https://doi.org/10.1061/\(ASCE\)GT.1943-5606.0000190](https://doi.org/10.1061/(ASCE)GT.1943-5606.0000190)
- Chlaib HK, Mahdi H, Al-Shukri H, Su MM, Catakli A, Abd N (2014) Using ground-penetrating radar in levee assessment to detect small-scale animal burrows. *J Appl Geophys* 103:121–131. <https://doi.org/10.1016/j.jappgeo.2014.01.011>
- Cleary PW, Prakash M, Mead S, Lemiale V, Robinson GK, Ye F, Ouyang S, Tang X (2015) A scenario-based risk framework for determining consequences of different failure modes of earth dams. *Nat Hazards* 75:1489–1530. <https://doi.org/10.1007/s11069-014-1379-x>
- Daniels DJ (2004) *Ground Penetrating Radar, seconded*. Institution of Engineering and Technology. https://books.google.hu/books?hl=en&lr=&id=16PV-fhKasoC&oi=fnd&pg=PR15&ots=u-bFZkV5rj&sig=8WN2SwUH6Z2KpJhOFya2G5wrDI&redir_esc=y#v=onepage&q&f=false
- Dezert T, Fargier Y, Palma Lopes S, Côte P (2019) Geophysical and geotechnical methods for fluvial levee investigation: a review. *Eng Geol* 260:105206. <https://doi.org/10.1016/j.enggeo.2019.105206>
- Di Prinzio M, Bittelli M, Castellarin A, Pisa PR (2010) Application of GPR to the monitoring of river embankments. *J Appl Geophys* 71(2–3):53–61. <https://doi.org/10.1016/j.jappgeo.2010.04.002>
- Fargier Y (2011) *Développement de l'Imagerie de Résistivité électrique pour la reconnaissance et la surveillance des Ouvrages Hydrauliques en Terre*. PhD thesis, Ecole Centrale de Nantes
- Fargier Y, Lopes SP, Fauchard C, François D, Côte, P., (2014) DC-Electrical Resistivity Imaging for embankment dike investigation: a 3D extended normalization approach. *J Appl Geophys* 103:245–256. <https://doi.org/10.1016/j.jappgeo.2014.02.007>
- François D, Mériaux P, Monnet J (2016) *Méthodologie de reconnaissance et de diagnostic de l'érosion interne des ouvrages hydrauliques en remblai*. Publications IREX, Presses des Ponts, Paris. OCLC: 966418274
- Gabris G, Nador A (2007) Long-term fluvial archives in Hungary: response of the Danube and Tisza rivers to tectonic movements and climatic changes during the Quaternary: a review and new synthesis. *Quatern Sci Rev* 26:2758–2782. <https://doi.org/10.1016/j.quascirev.2007.06.030>
- Geophysical Survry Systems Incorporation (GSSI) (2010) RADAN 7 software, accessible at: <https://www.geophysical.com/software>
- Guida RJ, Swanson TL, Remo JW, Kiss T (2015) Strategic floodplain reconnection for the Lower Tisza River, Hungary: Opportunities for flood-height reduction and floodplain-wetland reconnection. *J Hydrol* 521:274–285
- Grenerczy Gy, Farkas P, Frey S (2021) Ground motion map of Hungary (Version v20210322). Zenodo. <https://doi.org/10.5281/zenodo.4625653>


- Huang W-C, Weng M-C, Chen R-K (2014) Levee failure mechanisms during the extreme rainfall event: a case study in Southern Taiwan. *Nat Hazards* 70:1287–1307. <https://doi.org/10.1007/s11069-013-0874-9>
- Ihrig D (1973) A magyar vízszabályotás története (The history of Hungarian River Engineering). OVH, Budapest, p 398 (in Hungarian)
- Jodry C, Palma Lopes S, Fargier Y, Sanchez M, Côte P (2019) 2D-ERT monitoring of soil moisture seasonal behaviour in a river levee: a case study. *J Appl Geophys* 167:140–151. <https://doi.org/10.1016/j.jappgeo.2019.05.008>
- Jones G, Sentenac P, Zielinski M (2014) Desiccation cracking detection using 2-D and 3-D electrical resistivity tomography: validation on a flood embankment. *J Appl Geophys* 106:196–211
- Joó I (1996) Vertical surface movements in Hungary (A földfelszín magassági irányú mozgásai Magyarországon). *Geodézia És Kartográfia* 4:6–12 (in Hungarian)
- Karl L, Fechner T, François, S., and Degrande, G. (2008). Application of surface waves for the geotechnical characterisation of dykes. In: Near Surface 2008–14th EAGE European meeting of environmental and engineering geophysics
- Khalilzad M, Gabr MA (2011) Deformation-based limit states for earth embankments. In: Geo-Frontiers Congress, Dallas, Texas. [https://doi.org/10.1061/41165\(397\)372](https://doi.org/10.1061/41165(397)372)
- Khalilzad M, Gabr MA, Hynes ME (2014) Effects of woody vegetation on seepage-induced deformation and related limit state analysis of levees. *Int J Geomech* 14(2):302–312. [https://doi.org/10.1061/\(ASCE\)GM.1943-5622.0000304](https://doi.org/10.1061/(ASCE)GM.1943-5622.0000304)
- Khalilzad M, Gabr MA, Hynes ME (2015) Assessment of remedial measures to reduce exceedance probability of performance limit States in Embankment Dams. *Comput Geotech* 213–222. <https://doi.org/10.1016/j.comgeo.2015.02.010>
- Kiss T, Fiala K, Gy S, Szatmári G (2019) Long-term hydrological changes after various river regulation measures: are we responsible for flow extremes *Hydrol. Res* 50(2):417–430. <https://doi.org/10.2166/nh.2019.095>
- Kiss T, Hernesz P, Sipos G (2012) Meander cores on the floodplain the early Holocene development of the low-floodplain along the Lower Tisza Region, Hungary. *J Environ Geogr* 5:1–10. <https://doi.org/10.14232/jengeo-2012-43802>
- Kiss T, Hernesz P, Sümeghy B, Györgyövícs K, Gy S (2014) The evolution of the Great Hungarian Plain fluvial system—fluvial processes in a subsiding area from the beginning of the Weichselian. *Quatern Int* 388:142–155. <https://doi.org/10.1016/j.quaint.2014.05.050>
- Kiss T, Nagy J, Fehérvári I, Amissh GJ, Fiala K, Sipos G (2021) Increased flood height driven by local factors on a regulated river with a confined floodplain, Lower Tisza, Hungary. *Geomorphology* 389:107858. <https://doi.org/10.1016/j.geomorph.2021.107858>
- Knox RL, Morrison RR, Wohl EE (2022) Identification of artificial levees in the contiguous United States. *Water Resources Res.* <https://doi.org/10.1029/2021WR031308>
- Koncz I (2022) Oil and gas occurrences discovered in Hungary in period 1935 to 1985, and their features. *Földtani Közlelőny* 152(3):259–278. <https://doi.org/10.23928/foldt.kozl.2022.152.3.259>
- Kovács D (1979) Flood control, regulation of rivers and lakes and waterways in Hungary. National Water Management Authority (OVH), Budapest. <https://www.regikonyvek.hu/kiadas/arvizvedelem-folyo-es-toszabalyozas-vizutak-magyarorszagon-1979-vizugyi-dokumentacios-es-tovabbkepzo-intezt>
- Lászlóffy W (1982) The Tisza. Akadémiai Kiadó, Budapest, p 610 (in Hungarian)
- Lee B, Oh S, Yi MJ (2020) Mapping of leakage paths in damaged embankment using modified resistivity array method. *Eng Geol* 266:105469. <https://doi.org/10.1016/j.enggeo.2019.105469>
- Look BG (2014) Handbook of geotechnical investigation and design tables. CRC Press
- Lu N, Wu B, Tan CP (2007) Tensile strength characteristics of unsaturated sands. *J Geotech Geoenviron Eng* 133(2):144–154. [https://doi.org/10.1061/\(ASCE\)1090-0241\(2007\)133:2\(144\)](https://doi.org/10.1061/(ASCE)1090-0241(2007)133:2(144))
- Masannat YM (1980) Development of piping erosion conditions in the Benson area, Arizona, U.S.A. *Q J Eng Geol Hydrogeol* 13:53–61. <https://doi.org/10.1144/GSL.QJEG.1980.013.01.04>
- Mazzini E, Simoni G (2008) Relazione Descrittiva: Evento di Piena del 20 maggio 2008 del Torrente Samoggia. Regione Emilia-Romagna—Servizio Tecnico Bacino Reno (in Italian)
- Nagy L (2000) Az árvízvédelmi gátak geotechnikai problémái = Geotechnical problems of levees. *Vízügyi Közlemények* 82(1):121–146. (in Hungarian). https://adt.arcanum.com/hu/view/VizugyiKozlemenyek_2000/?pg=0&layout=s
- OVF (2014) Árvízi kockázati térképezés és stratégiai kockázatkezelési terv készítése (Flood risk mapping and strategic risk management plan), project report of the National Water Directorate Hungary, accessible at: http://www.vizugy.hu/vizstrategia/documents/B91A47EC-E3B8-4D58-A15F-3E522958BEE8/Orszagos_elontes_le_web.pdf

- Perri MT, Boaga J, Bersani S, Cassiani G, Cola S, Deiana R, Simonini P, Patti S (2014) River embankment characterisation: the joint use of geophysical and geotechnical techniques. *J Appl Geophys* 110:5–22. <https://doi.org/10.1016/j.jappgeo.2014.08.012>
- Radzicki K, Gołębowski T, Cwiklik M, Stoliński M (2021) A new levee control system based on geotechnical and geophysical surveys including active thermal sensing: A case study from Poland. *Eng Geol* 293:1. <https://doi.org/10.1016/j.enggeo.2021.106316>
- Rahimi S, Wood CM, Coker F, Moody T, Bernhardt-Barry M, Mofarraj Kouchaki B (2018) The combined use of MASW and resistivity surveys for levee assessment: a case study of the Melvin Price Reach of the Wood River Levee. *Eng Geol* 241(May):11–24. <https://doi.org/10.1016/j.enggeo.2018.05.009>
- Richards KS, Reddy KR (2010) New approach to assess piping potential in earth dams and levees. *ASCE News* 51(6):A1, A4, A5, and A10. https://www.researchgate.net/publication/297202931_New_Approach_to_Assess_Piping_Potential_in_Earth_Dams_and_Levees
- Upadhyay RK, Kishore N, Sharma M (2021) Delineation and mapping of palaeochannels using remote sensing, geophysical, and sedimentological techniques: A comprehensive approach. *Water Sci* 35(1):100–108. <https://doi.org/10.1080/23570008.2021.1941691>
- Ronai A (1985) Az Alföld negyedidőszaki földtana (Quaternary Geology of the Great Hungarian Plain). *Geologica Hungarica, Series Geologica* 21 (in Hungarian)
- Samyn K, Mathieu F, Bitri A, Nachbaur A, Closset L (2014) Integrated geophysical approach in assessing karst presence and sinkhole susceptibility along flood-protection dykes of the Loire River, Orléans, France *Eng Geol* 183:170–184. <https://doi.org/10.1016/j.enggeo.2014.10.013>
- Sandmeier (2016) Geophysical software—REFLEXW guide. Introduction to the processing of GPR-data within REFLEXW, 23p. https://www.sandmeier-geo.de/Download/gpr_2d_import_processing.pdf
- Sandmeier geophysical Software, 2016. Reflex 8.0. <http://www.sandmeier-geo.de/reflexw.html>.
- Schweitzer, F., 2002. A magyarországi folyószabályozások geomorfológiai vonatkozásai = Geomorphological aspects of Hungarian river regulation works. *Földrajzi értesítő* 50(1–4):63–72 (in Hungarian). <https://docplayer.hu/1721975-A-magyarorszag-i-folyoszabalyozasok-geomorfologiai-vonatkozasai.html>
- Seed RB, Bea RG, Abdelmalak RI, Athanasopoulos AG, Boutwell GP, Bray JD, Briaud J-L, Cheung C, Cobos-Roa D, Cohen-Waeber J, Collins BD, Ehrensing L, Farber D, Hanemann M, Harder LF, Inkabi KS, Kammerer AM, Karadeniz D, Kayen RE, Moss RES, Nicks J, Nimmala S, Pestana JM, Porter J, Rhee K, Riemer MF, Roberts K, Rogers JD, Storesund R, Govindasamy AV, Vera-Grunauer X, Wartman JE, Watkins CM, Wenk Jr E, Yim SC (2006) Investigation of the performance of the New Orleans flood protection systems in Hurricane Katrina on August 29, 2005. Volume I: Main Text and Executive Summary, Final Report, p 690. https://digitalcommons.calpoly.edu/cgi/viewcontent.cgi?article=1032&context=cenv_fac
- Sentenac P, Jones G, Zielinski M, Tarantino A (2012) An approach for the geophysical assessment of fissuring of estuary and river flood embankments: validation against two case studies in England and Scotland. *Environ Earth Sci*. <https://doi.org/10.1007/s12665-012-2026-z>
- Sentenac P, Benes V, Budinsky V, Keenan H, Baron R (2017) Post flooding damage assessment of earth dams and historical reservoirs using non-invasive geophysical techniques. *J Appl Geophys* 146:138–148. <https://doi.org/10.1016/j.jappgeo.2017.09.006>
- Sheishah D, Sipos G, Hegyi A, Kozák P, Abdelsamei E, Tóth C, Onaca A, Gergely Páll D (2022) Assessing the structure and composition of artificial levees along the lower Tisza River (Hungary). *Geographica Pannonica Journal* 26(3):258–272. <https://doi.org/10.5937/gp26-39474>
- Skelly RL, Bristow CS, Ethridge FG (2003) Architecture of channel-belt deposits in an aggrading shallow sandbed braided river: the lower Niobrara River, northeast Nebraska. *Sedimentary Geology*, 158(3–4), 249–270
- Słowik M (2012) Influence of measurement conditions on depth range and resolution of GPR images: The example of lowland valley alluvial fill (the Odra River, Poland). *J Appl Geophys* 85:1–14. <https://doi.org/10.1016/j.jappgeo.2012.06.007>
- Smith SS, Scullion T (1993) Development of ground-penetrating radar equipment for detecting pavement condition for preventive maintenance. Technical Report, Project H-104 A, Strategic Highway Research Program. Natural Resources Defense Council, Washington, DC, USA, p 177. <https://ui.adsabs.harvard.edu/abs/1993STIN...9511904S/abstract>

- Szűcs P, Nagy L, Ficsor J, Kovács S, Szlávik L, Tóth F, Keve G, Lovas A, Padányi J, Balatonyi L, Baross K, Sziebert J, Ficzer A, Göncz B, Dobó K (2019) Árvízvédelmi ismeretek = Flood Protection. <http://hdl.handle.net/20.500.12944/13490> (in Hungarian)
- Tanajewski D, Bakula M (2016) Application of Ground Penetrating Radar Surveys and GPS Surveys for Monitoring the Condition of Levees and Dykes. *Acta Geophys* 64(4):1093–1111. <https://doi.org/10.1515/acgeo-2016-0006>
- Tobin GA (1995) The levee love affair: a stormy relationship 1. *JAWRA J Am Water Resour Assoc* 31(3):359–367
- Tresoldi G, Arosio D, Hojat A, Longoni L, Papini M, Zanzi L (2019) Long-term hydrogeophysical monitoring of the internal conditions of river levees. *Eng Geol* 259:1039. <https://doi.org/10.1016/j.enggeo.2019.05.016>
- Utsi EC (2017) Ground penetrating radar theory and practice. In: *Ground Penetrating Radar Theory and Applications*. Butterworth-Heinemann publication Elsevier, 209 p. <https://www.scribd.com/book/345718688/Ground-Penetrating-Radar-Theory-and-Practice>
- USACE – U.S. Army Corps of Engineers (2000) EM 1110-2-1913, Engineering and Design—Design and Construction of Levees. Department of the Army, USACE, Washington, DC. https://www.yumpu.com/en/document/view/346990/departement-of-the-army-em-1110-2-1913-us-army-corps-of_
- Vandenbergh J, Van Overmeeren RA (1999) Ground penetrating radar images of selected fluvial deposits in the Netherlands. *Sed Geol* 128(3–4):245–270
- Wiscomb GW, Messmer TA (2010) Pocket Gophers. Utah State University Extension service and College of Natural Resources 6. https://digitalcommons.usu.edu/cgi/viewcontent.cgi?article=3303&context=wild_facpub
- Wei X, Gao C, Liu K (2020) A review of cracking behavior and mechanism in clayey soils related to desiccation. *Adv Civ Eng* 2020:19–27. <https://doi.org/10.1155/2020/8880873>
- Website 1: <https://education.nationalgeographic.org/resource/burrow>

Publisher's Note Springer Nature remains neutral with regard to jurisdictional claims in published maps and institutional affiliations.

Authors and Affiliations

Diaa Sheishah^{1,2} · Tímea Kiss¹ · Tibor Borza³ · Károly Fiala³ · Péter Kozák³ · Enas Abdelsamei^{1,2} · Csaba Tóth⁴ · Gyula Grenczy⁵ · Dávid Gergely Páll¹ · György Sipos¹ 

¹ Department of Geoinformatics, Physical and Environmental Geography, University of Szeged, Egyetem U. 2-6., 6722 Szeged, Hungary

² National Research Institute of Astronomy and Geophysics, El Marsad St., Helwan, Cairo 11421, Egypt

³ Lower Tisza District Water Directorate, Stefánia 4., 6720 Szeged, Hungary

⁴ Department of Highway and Railway Engineering, Budapest University of Technology and Economics, Műegyetem Rakpart 3., 1111 Budapest, Hungary

⁵ Geo-Sentinel Ltd., Kacsóh Pongrac U. 13., 2132 God, Hungary